PartCo: Part-Level Correspondence Priors Enhance Category Discovery

Fernando Julio Cendra   **Kai Han**[*]

Visual AI Lab, The University of Hong Kong
fcendra@connect.hku.hk   kaihanx@hku.hk

Abstract

Generalized Category Discovery (GCD) aims to identify both known and novel categories within unlabeled data by leveraging a set of labeled examples from known categories. Existing GCD methods primarily depend on semantic labels and global image representations, often overlooking the detailed part-level cues that are crucial for distinguishing closely related categories. In this paper, we introduce PartCo, short for Part-Level Correspondence Prior, a novel framework that enhances category discovery by incorporating part-level visual feature correspondences. By leveraging part-level relationships, PartCo captures finer-grained semantic structures, enabling a more nuanced understanding of category relationships. Importantly, PartCo seamlessly integrates with existing GCD methods without requiring significant modifications. Our extensive experiments on multiple benchmark datasets demonstrate that PartCo significantly improves the performance of current GCD approaches, achieving state-of-the-art results by bridging the gap between semantic labels and part-level visual compositions, thereby setting new benchmarks for GCD. Project page: https://visual-ai.github.io/partco

1 Introduction

Supervised deep learning models have fundamentally transformed computer vision, showcasing exceptional proficiency in classifying predefined image categories. Models trained on extensive labeled datasets achieve high accuracy and robustness in distinguishing known classes within controlled environments. However, their performance significantly diminishes when confronted with samples from categories that were neither present nor represented during training. This limitation impedes the deployment of intelligent systems in dynamic, real-world scenarios where encountering previously unseen categories is inevitable. To address this challenge, Generalized Category Discovery (GCD) (Vaze et al., 2022a) has emerged as a pivotal task. As depicted in Fig. 1, GCD aims to automatically identify and categorize both known and novel classes within unlabeled data by leveraging a modest set of labeled examples from known categories. Unlike traditional supervised learning, which operates within a rigid framework of predefined categories, GCD extends the model's capability to recognize and incorporate novel, unseen categories alongside known ones.

Figure 1: **Generalized Category Discovery:** Given a labeled subset contains seen classes, the task is to categorize the unlabeled images, which may belong to seen or unseen classes.

A growing body of literature in GCD emphasizes the significance of object parts as effective conduits for transferring knowledge between "seen" and "unseen" categories (Vaze

---

[*]Corresponding author.

et al., 2022a; Wang et al., 2024). Object parts encapsulate fine-grained visual features that are often shared across different categories, facilitating the generalization to novel classes.

However, recent approaches predominantly rely on global representations derived from the classification token of transformer-based models. While these global features capture the overall semantic content of an image, they inherently abstract away detailed part-level information, which is vital for distinguishing closely related categories. For instance, Wang et al. (2024) introduces a spatial prompt tuning method that learns pixel-level prompts around local image regions to incorporate part-level information. Although innovative, this method does not account for the inherent variability in object parts, such as differing scales, orientations, or varying numbers of parts due to occlusions (Fig. 2). This motivates an explicit part-aware prior that is robust to scale, pose, and occlusion.
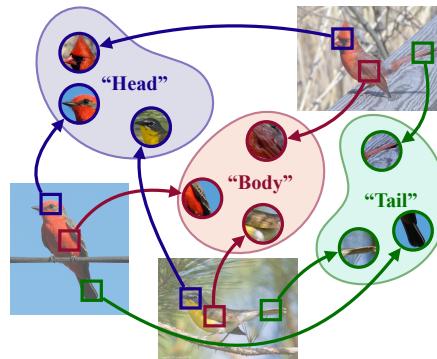

Figure 2: **Part variability.** Parts (head, body, tail) vary in scale, pose, and visibility yet still correspond across images, motivating part-aware priors beyond global features.

Vision Transformer (ViT) models, in addition to the classification token, incorporate patch tokens that encapsulate high-dimensional features for each image patch. These patch tokens inherently contain part-level observations, offering a granular perspective of the image's composition. However, directly utilizing these patch tokens presents several challenges: the absence of explicit part-level information, the presence of foreground-background noise, and varying object scales and orientations across samples. These issues necessitate an effective *supervisory signal* to fully harness the potential of patch token representations in ViT models.

Recent advancements in self-supervised vision foundation models, particularly the ViT-based DINO variants (Caron et al., 2021; Oquab et al., 2024; Siméoni et al., 2025), have demonstrated remarkable generalizability across various tasks. These models excel at extracting high-dimensional patch token features that capture detailed and localized semantic information for each image patch. Unlike the classification token, which summarizes the entire image, patch tokens focus on specific parts, providing a more detailed view of the image's composition. Importantly, these enhanced feature descriptors inherently provide the necessary part-level correspondence labels, serving as an ideal supervisory signal for leveraging patch tokens within the GCD framework.

To address these challenges, we propose *PartCo*, short for **Part**-Level **Co**rrespondence Prior, a versatile framework designed to introduce part-level correspondence labels into the GCD process. By explicitly guiding ViT patch token features with these correspondence labels, PartCo better leverages the utilization of the model's rich feature representations. Additionally, we introduce a novel part-level correspondence loss that effectively leverages these part-level features, ensuring that detailed object part information is accurately captured and utilized for category discovery. Through comprehensive evaluations on both fine-grained and generic benchmark datasets, PartCo achieves state-of-the-art (SOTA) performance, setting a new standard for the GCD task.

2 PRELIMINARIES

Problem statement. Generalized Category Discovery (GCD) aims to develop a model that accurately classifies unlabeled samples from known categories while simultaneously clustering those from novel, unseen categories. Consider an unlabeled dataset $\mathbf{D}_u = \{(\mathbf{x}_i^u, y_i^u)\} \subset \mathbf{X} \times \mathbf{Y}_u$ and a labeled dataset $\mathbf{D}_l = \{(\mathbf{x}_i^l, y_i^l)\} \subset \mathbf{X} \times \mathbf{Y}_l$, where $\mathbf{Y}_u$ and $\mathbf{Y}_l$ represent the label sets for unlabeled and labeled data, respectively. The unlabeled dataset contains samples from both known categories (included in $\mathbf{Y}_l$) and unknown categories, specifically $\mathbf{Y}_l \subset \mathbf{Y}_u$. Let $M = |\mathbf{Y}_l|$ denote the number of labeled categories. We assume the total number of categories, $K = |\mathbf{Y}_l \cup \mathbf{Y}_u|$, is known, as established in prior studies (Han et al., 2021; Vaze et al., 2023). When this information is unavailable, methods such as those in Han et al. (2019); Vaze et al. (2022a) can provide reliable estimates.

Baselines. The *non-parametric* baseline (Vaze et al., 2022a; Rastegar et al., 2024) for GCD is introduced by fine-tuning the pre-trained DINO model (Caron et al., 2021; Dosovitskiy et al., 2021). The loss function generally integrates both self-supervised and supervised contrastive losses. For two augmented views $\mathbf{x}_i$ and $\mathbf{x}'_i$ over a mini-batch B, we obtain ℓ_2-normalized features $\mathbf{z}_i = \psi(\phi(\mathbf{x}_i))$ and $\mathbf{z}'_i = \psi(\phi(\mathbf{x}'_i))$, where ϕ is the backbone and ψ is the projection head; τ_r denotes the temperature parameter. The contrastive losses are then defined as:

$$\mathcal{L}^u_{rep} = \frac{1}{|B|} \sum_{i \in B} -\log \frac{\exp(\mathbf{z}_i \cdot \mathbf{z}'_i / \tau_r)}{\sum_{j \neq i} \exp(\mathbf{z}_i \cdot \mathbf{z}'_j / \tau_r)}, \quad \mathcal{L}^s_{rep} = \frac{1}{|B_l|} \sum_{i \in B_l} \frac{1}{|\mathbb{N}_i|} \sum_{q \in \mathbb{N}_i} -\log \frac{\exp(\mathbf{z}_i \cdot \mathbf{z}_q / \tau_r)}{\sum_{j \neq i} \exp(\mathbf{z}_i \cdot \mathbf{z}_j / \tau_r)}. \tag{1}$$

Here, $\mathbb{N}_i$ contains indices of labeled samples sharing the same label y^l_i as $\mathbf{x}_i$. The total representation loss $\mathcal{L}_{rep}$ is a weighted combination:

$$\mathcal{L}_{rep} = (1 - \lambda_b)\mathcal{L}^u_{rep} + \lambda_b \mathcal{L}^s_{rep}, \tag{2}$$

where λ_b is the balancing factor.

The *parametric* baseline from (Wen et al., 2023) employs a parametric classifier within a self-distillation framework (Caron et al., 2021). Initialized with K normalized category prototypes $\mathbf{L} = \{\mathbf{l}_1, \ldots, \mathbf{l}_K\}$, the classifier computes the probability for category k as:

$$\mathbf{p}^{(k)}_i = \frac{\exp(\mathbf{o}_i \cdot \mathbf{l}_k / \tau_s)}{\sum_{j=1}^{K} \exp(\mathbf{o_i} \cdot \mathbf{l}_j / \tau_s)}, \tag{3}$$

where $\mathbf{o}_i = \phi(\mathbf{x}_i) / \|\phi(\mathbf{x}_i)\|$ and τ_s is the student temperature. Soft labels $\mathbf{q}_i$ are generated by a teacher network with temperature τ_t. The unsupervised classification loss $\mathcal{L}^u_{cls}$ is defined as $\mathcal{L}^u_{cls} = \frac{1}{|B|} \sum_{i \in B} \ell_{ce}(\mathbf{q}'_i, \mathbf{p}_i) - \xi\mathcal{H}(\overline{\mathbf{p}})$, where $\overline{\mathbf{p}} = \frac{1}{2|B|} \sum_{i \in B}(\mathbf{p}_i + \mathbf{p}'_i)$ denotes the mean prediction across the mini-batch, ℓ_{ce} is the cross-entropy loss and $\mathcal{H}$ is the mean entropy, weighted by ξ. For labeled samples, the supervised loss $\mathcal{L}^s_{cls} = \frac{1}{|B_l|} \sum_{i \in B_l} \ell_{ce}(\mathbf{p}_i, \mathbf{y}_i)$ is used. The overall classification loss combines unsupervised and supervised components as: $\mathcal{L}_{cls} = (1 - \lambda_b)\mathcal{L}^u_{cls} + \lambda_b \mathcal{L}^s_{cls}$. Finally, integrating with the non-parametric representation loss in Eq. 2 yields the comprehensive GCD objective:

$$\mathcal{L}_{\text{gcd}} = \mathcal{L}_{cls} + \mathcal{L}_{rep}. \tag{4}$$

Limitation of baselines. Although the non-parametric and parametric baselines obtain encouraging results on GCD, they exhibit significant limitations. Primarily, these methods rely solely on the foundation model's classification token (`[CLS]`) representation, which captures only global information about the input data. This exclusive dependence on global representations restricts the models from leveraging part-level or localized information that is essential for distinguishing fine-grained categories. Without incorporating detailed, part-specific features, the baselines may overlook subtle patterns and contextual nuances within the data, leading to less effective performance in category discovery.

3 PART-LEVEL CORRESPONDENCE PRIOR (PARTCO) FRAMEWORK

Building upon the motivations outlined in the introduction, we introduce *PartCo*, a novel framework meticulously crafted to harness part-level information from ViT's patch tokens for GCD. Unlike traditional approaches that rely solely on global representations provided by the `[CLS]` token, PartCo fully leverages the rich, high-dimensional features embedded within ViT's patch tokens. By generating and utilizing explicit part-level correspondence labels, PartCo effectively bridges the gap between coarse global features and fine-grained local details. Furthermore, this design allows PartCo to be seamlessly integrated into existing GCD methods, enhancing their performance without necessitating significant modifications.

By making use of these part-level correspondence labels, PartCo fully utilizes the vision foundation model beyond just the `[CLS]` token. These labels act as robust supervisory signals, guiding the patch token features to focus on meaningful object parts and mitigating common challenges such as foreground-background noise and variability in object scales and orientations. This guidance enables the full potential of vision foundation models to be realized, ensuring that both global and local feature representations are explicitly integrated into the GCD process. In the subsequent sections, we detail the construction and utilization of part-level correspondence labels within the PartCo framework.

3.1 CONSTRUCTING PART-LEVEL CORRESPONDENCE LABELS

To construct part-level correspondence labels, we employ a two-step process, illustrated in Fig. 3, leveraging the rich feature representations from the frozen DINOv2 model. This approach ensures robust label inference across both labeled and unlabeled samples by first acquiring relevant PCA projections and then assigning labels through k-means clustering.
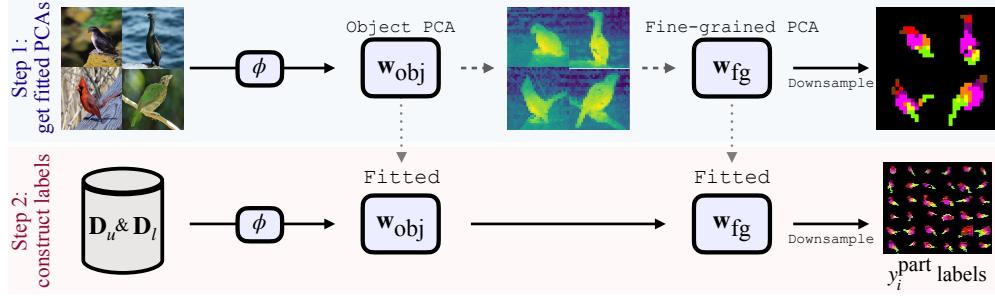

Figure 3: **Overview of part-level correspondence labels construction:** This two-step process begins by applying PCA projections to extract object and detailed features from ViT's patch tokens using a subset of the dataset. These projections are then applied to the entire dataset to generate part-level correspondence labels.

Step 1: PCA projections. We begin by sampling a subset of M labeled images from the dataset $\mathbf{D}_l$, ensuring that each sample represents a distinct category. From these images, we extract their patch token features denoted as $\mathbf{F} \in \mathbb{R}^{M \times N \times d}$ using vision foundation model ϕ, *e.g.*, DINO backbone (Oquab et al., 2024; Siméoni et al., 2025), where N is the number of patch tokens and d is the feature dimension. The first principal component analysis (PCA) is applied to $\mathbf{F}$ to obtain the primary projection vector $\mathbf{w}_{\text{obj}} \in \mathbb{R}^d$, which captures the most significant variation corresponding to object regions: $\mathbf{w}_{\text{obj}} = \text{argmax}_{\mathbf{w}} \frac{\mathbf{w}^\top \mathbf{F}^\top \mathbf{F} \mathbf{w}}{\mathbf{w}^\top \mathbf{w}}$. Using this projection, we compute the objectness score for each patch: $\mathbf{F}_{\text{obj}} = \mathbf{F} \cdot \mathbf{w}_{\text{obj}}$, and generate a binary mask $\mathbf{M}$ by thresholding at $\tau_{\text{obj}} = 0.6$: $\mathbf{M} = \mathbb{1}(\mathbf{F}_{\text{obj}} > \tau_{\text{obj}})$. This mask distinguishes foreground patches from background ones. Subsequently, we perform a second PCA on the masked features to extract fine-grained information. Specifically, we compute the element-wise multiplication $\mathbf{F} \odot \mathbf{M}$ and apply PCA to obtain the projection matrix $\mathbf{w}_{\text{fg}} \in \mathbb{R}^{d \times 3}$, resulting in the fine-grained feature representation: $\mathbf{F}_{\text{fg}} = (\mathbf{F} \odot \mathbf{M}) \cdot \mathbf{w}_{\text{fg}}$. This transformation maps the first three components of the PCA computed over the feature space to RGB.

Step 2: Label construction. We determine the optimal number of part-level labels, k^*, by applying k-means clustering to the normalized fine-grained features $\mathbf{F}_{\text{fg}}$. Each clustering solution is evaluated based on two criteria: (1) *minimum distance* between cluster centers to ensure that the clusters are well separated, reducing overlap and increasing distinctiveness. (2) *balance of cluster sizes*: prevents skewed distributions where some clusters dominate over others, promoting uniformity. We sweep k over a candidate set and select k^* by maximizing $\min_{i \neq j} \|\mathbf{c}_i - \mathbf{c}_j\| \times (\min_i |C_i| / \max_j |C_j|)$, favoring well-separated and balanced clusters. Here, $\mathbf{c}_i$ and $\mathbf{c}_j$ denote the centroids of clusters i and j, and $|C_i|$ is the number of samples in cluster i. With k^* fixed, we assign part-level correspondence labels to all samples in $\mathbf{D}$. We then define the part label map $y_i^{\text{part}} \in \{1, \ldots, k^*\}$ with resolution following ViT's patch token size as:

$$y_i^{\text{part}} = \arg\min_{\mathbf{c} \in \mathcal{C}} \|\mathbf{F}_{\text{fg}} - \mathbf{c}\|, \tag{5}$$

where $\mathcal{C} = \{\mathbf{c}_1, \mathbf{c}_2, \ldots, \mathbf{c}_{k^*}\}$ represents the set of optimal cluster centers from k-means. We refer to these as *1st order part-level correspondence labels*.

Enhancing granularity in part-level correspondence. While 1st order part-level labels are adequate for fine-grained datasets due to the presence of shared superclasses, they may be too general for generic datasets lacking such similarities as shown in Fig. 4. To capture more intricate details in these cases, we introduce *2nd order part-level correspondence labels*. This process involves applying an additional PCA on the fine-grained features $\mathbf{F}_{\text{fg}}$ within each 1st order cluster. By doing so, we identify finer distinctions within each part, uncovering common features among similar but distinct parts. This 2nd order of labeling increases the granularity of part-level correspondence, enabling more
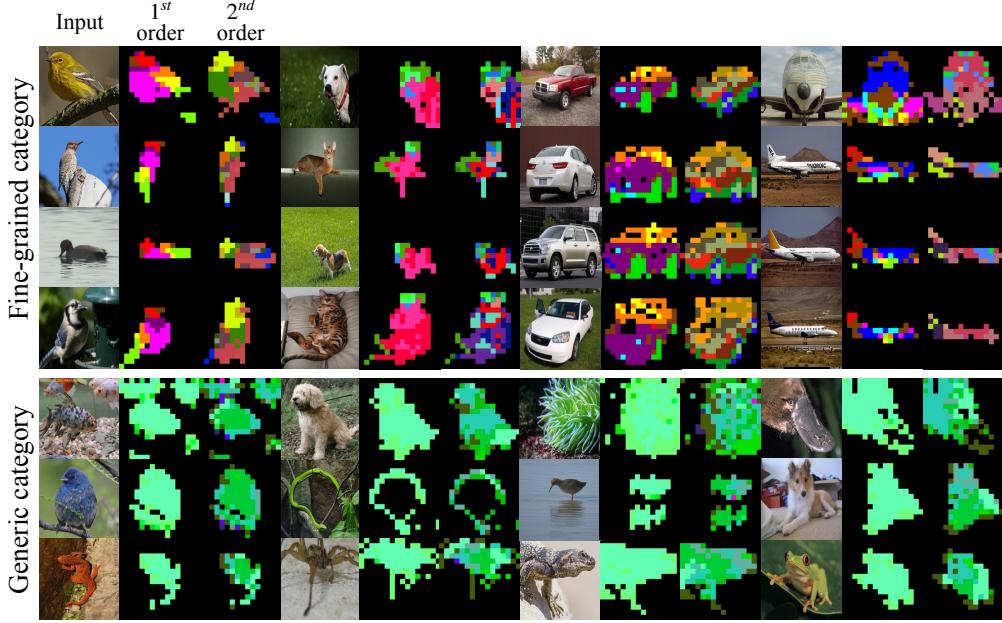
Figure 4: **Visualization of our part-level correspondence labels.** For each image, we generate both first- and second-order labels. First-order labels suffice for fine-grained datasets, while second-order labels capture additional detail for generic datasets. In practice, selecting between 1st- and 2nd-order is straightforward: datasets with subtle, intra-class differences indicate fine-grained samples, whereas datasets with pronounced, inter-class differences indicate generic samples.

precise category discovery in generic datasets where parts exhibit greater diversity and require finer resolution to discern subtle differences. We provide more discussion on our design choice of PCA + DINO patch descriptors and alternatives in Sec. S2.2 of the supplementary.

3.2 INTEGRATING PARTCO FRAMEWORK WITH GCD METHOD

After obtaining part-level correspondence labels, as explained in Section 3.1, we incorporate the PartCo framework, illustrated in Fig. 5 (a), into existing GCD methods. This integration is achieved through the introduction of a part-level correspondence loss $\mathcal{L}_{pc}$, which supervises the aggregated part features derived from patch tokens, thereby fostering robust part-level relationships within the ViT's feature representations.

(a) PartCo framework

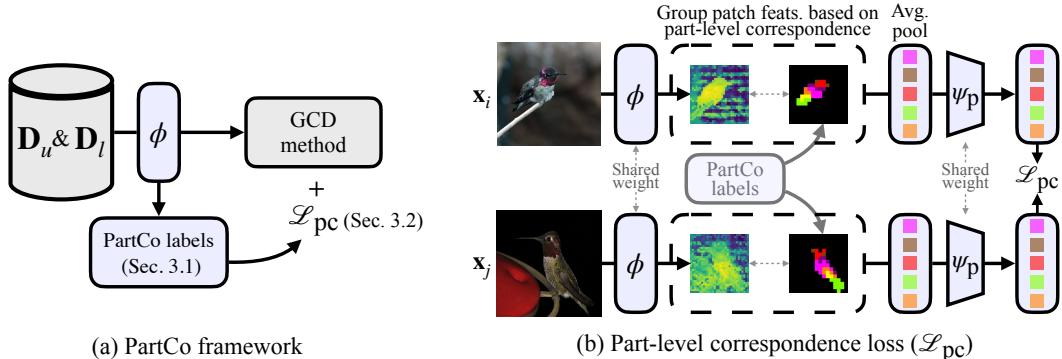(b) Part-level correspondence loss ($\mathcal{L}_{pc}$)

Figure 5: **(a) PartCo framework:** Introduces part-level correspondence labels as a plug-and-play module to enhance GCD methods. **(b) Part-level correspondence loss:** Depicts how part-level correspondence loss is integrated into the model to learn relationships between parts in ViT's patch token features.

Guiding patch token features. For an input image $\mathbf{x}_i$, we first extract its patch token features using the foundation model ϕ, yielding $\mathbf{F}_i = \phi(\mathbf{x}_i) \in \mathbb{R}^{N \times d}$. Utilizing the corresponding part-level

correspondence labels y_i^{part}, we organize the patch features based on their assigned part categories. Specifically, for each part category $c \in \mathcal{C}$ (where $\mathcal{C}$ represents the set of all part-level categories), we aggregate the features of patches labeled as c by computing their average: $\mathbf{f}_c = \frac{1}{|\mathcal{P}_c|} \sum_{j \in \mathcal{P}_c} \mathbf{F}_{i,j}$, where $\mathcal{P}_c = \{j \mid y_i^{\text{part}}(j) = c\}$ denotes the set of patch indices corresponding to part category c. This pooling operation results in a set of aggregated part-level features $\{\mathbf{f}_c\}_{c \in \mathcal{C}}$, each encapsulating the information of a specific part within the image. To further refine these aggregated features, we employ a part projection head ψ_p, which projects each aggregated feature $\mathbf{f}_c$ into a new feature space: $\mathbf{h}_c = \psi_{\mathrm{p}}(\mathbf{f}_c)$, where $\mathbf{h}_c \in \mathbb{R}^{d'}$ represents the projected feature for part category c, and d' is the dimensionality of the projected feature space. The projection head ψ_{p} is typically implemented as a multi-layer perceptron (MLP) that maps the aggregated features to a space optimized for contrastive learning. The overview of the process is shown in Fig. 5 (b).

Part-level correspondence loss. To effectively leverage these projected part-level features, we introduce a supervised part contrastive loss $\mathcal{L}_{\text{pc}}^{\text{sup}}$ that operates on the labeled data $\mathbf{D}_l$. This loss encourages features of the same part type and class to be close while separating different parts and/or classes, thereby enhancing the discriminative capability of the model at the part level. Formally, for a batch of B_l labeled samples, the supervised contrastive loss is defined as:

$$\mathcal{L}_{\text{pc}}^{\text{sup}} = \frac{1}{|B_l|} \sum_{i \in B_l} \frac{1}{|\mathcal{C}|} \sum_{c \in \mathcal{C}} \frac{1}{|\mathbb{N}_i^c|} \sum_{q \in \mathbb{N}_i^c} -\log \frac{\exp(\mathbf{h}_c \cdot \mathbf{h}_q / \tau_r)}{\sum_{j \notin \mathbb{N}_i^c} \exp(\mathbf{h}_c \cdot \mathbf{h}_j / \tau_r)}, \tag{6}$$

where $\mathbb{N}_i^c$ contains indices of labeled samples sharing the same label y_i^l and part category c as $\mathbf{x}_i$. This loss function ensures that projected features $\mathbf{h}_c$ of the same part type and category are drawn closer in the feature space, while those of different part type and categories are repelled, thereby fostering more discriminative part-specific representations.

For parametric baselines that incorporate pseudo-labels, in Eq. 3, for unlabeled data $\mathbf{D}_u$, we extend the part-level correspondence loss to include an unsupervised part contrastive loss $\mathcal{L}_{\text{pc}}^{\text{unsup}}$. This loss operates similarly to its supervised counterpart but utilizes pseudo-labels $\mathbf{p}_i$ generated by the model.

$$\mathcal{L}_{\text{pc}}^{\text{unsup}} = \frac{1}{|B_u|} \sum_{i \in B_u} \frac{1}{|\mathcal{C}|} \sum_{c \in \mathcal{C}} \frac{1}{|\mathbb{M}_i^c|} \sum_{q \in \mathbb{M}_i^c} -\log \frac{\exp(\mathbf{h}_c \cdot \mathbf{h}_q / \tau_r)}{\sum_{j \notin \mathbb{M}_i^c} \exp(\mathbf{h}_c \cdot \mathbf{h}_j / \tau_r)}, \tag{7}$$

where $\mathbb{M}_i^c$ contains indices of unlabeled samples sharing the same pseudo label and part category as $\mathbf{x}_i$. This unsupervised loss complements the supervised loss, enabling the model to learn from both labeled and unlabeled data effectively.

Overall training objective. The integration of the PartCo framework with existing GCD methods is formalized by combining the GCD's baseline loss in Eq. 4 with the newly introduced part-level correspondence loss. The final training objective is given by:

$$\mathcal{L}_{\text{total}} = \mathcal{L}_{\text{gcd}} + \mathcal{L}_{\text{pc}}, \tag{8}$$

where $\mathcal{L}_{\text{pc}} = (1 - \lambda_b)\mathcal{L}_{\text{pc}}^{\text{unsup}} + \lambda_b \mathcal{L}_{\text{pc}}^{\text{sup}}$ for parametric baselines, or $\mathcal{L}_{\text{pc}} = \lambda_b \mathcal{L}_{\text{pc}}^{\text{sup}}$ for non-parametric ones. By incorporating $\mathcal{L}_{\text{pc}}$, the model utilizes both global features from the `[CLS]` token and detailed part-specific features from the patch tokens. This dual supervision enhances the model's ability to discover and distinguish categories with finer details.

4 EXPERIMENTS

In this section, we describe our experimental setups in Sec. 4.1. Next, we present our main results in Sec. 4.2. Finally, in Sec. 4.3 we analyze the effectiveness of our model's components and design choices.

4.1 EXPERIMENTAL SETUP

Datasets. We evaluate our method using several benchmark datasets. Specifically, we use the Semantic Shift Benchmark (SSB) (Vaze et al., 2022b), which includes fine-grained datasets: Caltech-UCSD Birds-200-2011 (CUB) (Wah et al., 2011), Stanford Cars (Krause et al., 2013), and FGVC-Aircraft (Maji et al., 2013). Additionally, we employ generic benchmark datasets:

CIFAR10 (Krizhevsky & Hinton, 2009), CIFAR100 (Krizhevsky & Hinton, 2009), and ImageNet-100 (Deng et al., 2009). For each dataset, we utilize the data partitioning strategy specified in (Vaze et al., 2022a). This approach involves selecting a subset of all classes as the known ('Old') classes, denoted by $\mathbf{Y}_l$. Subsequently, 50% of the images from these known classes are allocated to the labeled dataset $\mathbf{D}_l$, and the remaining images are designated as the unlabeled dataset $\mathbf{D}_u$. Detailed statistics of the datasets are provided in Tab. A, supp. material.

Evaluation metrics. We assess the performance of our approach using clustering accuracy (*ACC*; Hungarian-matched), as defined in the existing literature (Vaze et al., 2022a). The *ACC* for the unlabeled dataset $\mathbf{D}_u$ is calculated based on the ground-truth labels y_i^u and the predicted labels $\hat{y}_i^u$ using the following equation:

$$ACC = \frac{1}{|\mathbf{D}_u|} \sum_{i=1}^{|\mathbf{D}_u|} \mathbb{1}(y_i^u = h(\hat{y}_i^u)), \tag{9}$$

where h represents the optimal permutation that aligns the predicted cluster assignments with the true labels. Additionally, we report the *ACC* values separately for the 'All', 'Old', and 'New' classes to provide a detailed evaluation of the model's performance across different category groups.

Implementation details. We integrate our PartCo framework with the widely used parametric model SimGCD (Wen et al., 2023) and the SOTA non-parametric GCD method SelEx (Rastegar et al., 2024), employing DINO-variants (Oquab et al., 2024; Siméoni et al., 2025) pretrained weights. For SimGCD (Wen et al., 2023), the feature dimension from the backbone ϕ is set to 768. The projection head ψ, the part projection head ψ_p and the final block of ϕ are optimized using the SGD optimizer with an initial learning rate of 0.1, which decays to 0.001 following a cosine annealing schedule, and the balancing factor λ_b is fixed at 0.35. Both models are trained for 200 epochs with a batch size of 128. All input images are resized to 224×224 and augmented to match the DINO pretrained model settings. All results are on a single NVIDIA RTX 4090; PartCo adds no inference cost. The part-level label construction takes around 5–180 min depending on dataset size (Tab. A, supp. material).

Comparison with other methods. We compare our method with other representative and SOTA GCD methods: 1) GCD (Vaze et al., 2022a); 2) SimGCD (Wen et al., 2023); 3) μGCD (Vaze et al., 2023); 4) AMEND (Banerjee et al., 2024); 5) CiPR (Hao et al., 2024); 6) SPTNet (Wang et al., 2024); 7) ProtoGCD (Ma et al., 2025); 8) FlipClass (Lin et al., 2024); and 9) SelEx (Rastegar et al., 2024). We also report k-means clustering results on frozen DINO (Oquab et al., 2024; Siméoni et al., 2025).

4.2 EXPERIMENTAL RESULTS

Benchmark results. Tab. 1 and 2 report per-dataset results on SSB (fine-grained) and on generic datasets. PartCo consistently improves the parametric model SimGCD and the non-parametric model SelEx, using DINO variants, achieving SOTA results. Unless stated otherwise, all "% gains" below denote *absolute* differences in *ACC*. On SSB, in terms of overall 'All' *ACC* across datasets (Fig. 6), PartCo-SimGCD improves by +9.8% with DINOv2 and +3.8% with DINOv3; PartCo-SelEx improves by +2.4% and +2.9%, respectively. On generic datasets, the gains are +0.3%/+0.9% for PartCo-SimGCD and +2.2%/+1.0% for PartCo-SelEx (v2/v3).
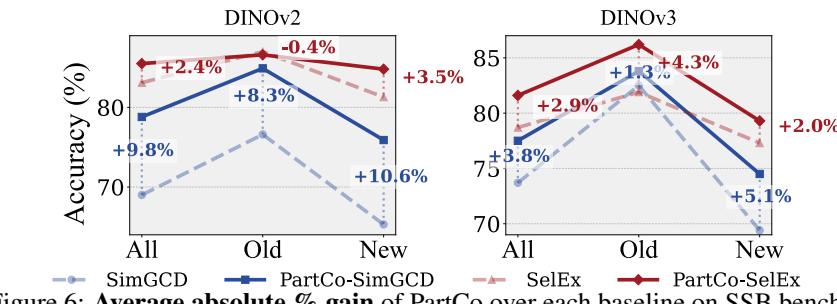

Figure 6: **Average absolute % gain** of PartCo over each baseline on SSB benchmark.

On SSB per-dataset results, we observe large *absolute* % gains across all three datasets: FGVC-Aircraft (DINOv2: +12.6%, DINOv3: +3.9%), CUB (DINOv2: +9.6%, DINOv3: +2.9%), and Stanford-Cars (DINOv2: +7.4%, DINOv3: +4.6%). On generic per-dataset results, gains are smaller but steady. These trends are consistent across DINOv2 and DINOv3, and PartCo integration consistently boosts GCD methods, yielding new state-of-the-art results across diverse datasets.

Table 1: Comparison of GCD methods on the SSB benchmark datasets. Results are reported in *ACC* across the 'All', 'Old' and 'New' categories.

Method	Backbone	CUB			Stanford-Cars			FGVC-Aircraft			Average		
		All	Old	New	All	Old	New	All	Old	New	All	Old	New
k-means	DINOv2	67.6	60.6	71.1	29.4	24.5	31.8	18.9	16.9	19.9	38.6	34.0	40.0
GCD	DINOv2	71.9	71.2	72.3	65.7	67.8	64.7	55.4	47.9	59.2	64.3	62.3	65.4
μGCD	DINOv2	74.0	75.9	73.1	76.1	91.0	68.9	66.3	68.7	65.1	72.1	78.6	69.0
CiPR	DINOv2	78.3	73.4	80.8	66.7	77.0	61.8	-	-	-	-	-	-
SPTNet	DINOv2	76.3	79.5	74.6	-	-	-	-	-	-	-	-	-
ProtoGCD	DINOv2	75.7	81.5	72.9	77.6	90.5	71.5	71.1	76.3	68.5	74.8	82.7	71.0
FlipClass	DINOv2	79.3	80.7	78.5	78.0	88.0	73.2	71.1	75.1	69.1	76.1	81.3	73.6
SimGCD	DINOv2	71.5	78.1	68.3	71.5	81.9	66.6	63.9	69.9	60.9	69.0	76.6	65.3
PartCo-SimGCD (**Ours**)	DINOv2	81.1	82.4	80.5	78.9	91.5	72.8	76.5	80.9	74.4	78.8	84.9	75.9
SelEx	DINOv2	87.4	**85.1**	88.5	82.2	**93.7**	76.7	79.8	82.3	78.6	83.1	**87.0**	81.3
PartCo-SelEx (**Ours**)	DINOv2	**90.6**	84.5	**93.2**	**82.5**	91.8	**78.0**	**83.4**	83.6	**83.3**	**85.5**	86.6	**84.8**
k-means	DINOv3	69.8	64.7	72.3	59.0	50.8	63.1	40.3	35.3	42.8	56.4	50.3	59.4
SimGCD	DINOv3	75.9	83.8	72.0	73.9	79.4	71.3	71.4	**84.4**	65.0	73.7	82.5	69.4
PartCo-SimGCD (**Ours**)	DINOv3	78.8	83.4	76.6	78.5	86.5	74.6	75.3	81.6	72.2	77.5	83.8	74.5
SelEx	DINOv3	83.5	78.1	86.2	78.8	90.3	73.3	73.9	77.3	72.4	78.7	81.9	77.3
PartCo-SelEx (**Ours**)	DINOv3	**86.1**	84.4	**87.0**	**81.7**	92.1	76.6	**76.9**	82.2	74.2	**81.6**	86.2	79.3

Table 2: Comparison of GCD methods on the generic benchmark datasets. Results are reported in *ACC* across the 'All', 'Old' and 'New' categories.

Method	Backbone	CIFAR10			CIFAR100			ImageNet-100			Average		
		All	Old	New	All	Old	New	All	Old	New	All	Old	New
k-means	DINOv2	94.9	95.2	94.8	70.9	70.8	72.1	78.3	80.5	77.2	81.4	82.2	81.4
GCD	DINOv2	97.8	99.0	97.1	79.6	84.5	69.9	78.5	89.5	73.0	85.3	91.0	80.0
AMEND	DINOv2	97.7	96.6	98.3	83.5	83.0	84.5	87.3	95.1	83.4	89.5	91.6	88.7
CiPR	DINOv2	99.0	98.7	99.2	90.3	89.0	93.1	88.2	87.6	88.5	92.5	91.8	93.6
SPTNet	DINOv2	-	-	-	-	-	-	90.1	96.1	87.1	-	-	-
FlipClass	DINOv2	99.0	98.2	99.4	91.7	90.4	94.2	91.0	96.3	88.3	93.9	95.0	94.0
SimGCD	DINOv2	98.7	96.7	**99.7**	88.5	89.2	87.2	89.9	95.5	87.1	92.4	93.8	91.3
PartCo-SimGCD (**Ours**)	DINOv2	99.0	98.7	99.2	89.0	92.0	83.0	90.1	92.0	89.2	92.7	94.2	90.4
SelEx	DINOv2	98.5	98.8	98.5	87.7	90.8	81.5	90.9	96.2	88.3	92.4	95.3	89.4
PartCo-SelEx (**Ours**)	DINOv2	**99.2**	**99.4**	98.9	90.0	92.8	84.3	**94.5**	**97.8**	**92.8**	**94.6**	**96.7**	92.0
k-means	DINOv3	94.1	95.1	93.6	65.5	66.4	63.5	78.3	78.3	78.3	79.3	79.9	78.5
SimGCD	DINOv3	98.4	98.7	98.2	84.3	88.3	74.3	92.2	96.5	90.0	91.6	94.8	87.5
PartCo-SimGCD (**Ours**)	DINOv3	**98.9**	98.2	**99.3**	85.0	88.9	77.1	93.7	96.5	92.3	92.5	94.5	89.6
SelEx	DINOv3	98.2	99.0	97.7	87.7	88.7	85.7	93.4	96.9	91.6	93.1	94.9	91.6
PartCo-SelEx (**Ours**)	DINOv3	98.3	**99.1**	97.9	**90.2**	91.7	87.0	93.8	96.6	92.4	**94.1**	95.8	92.4

4.3 MODEL COMPONENT ANALYSIS

Effectiveness of 1st vs. 2nd order part-level correspondence labels. We conduct an ablation study within our PartCo framework to compare 1st, and 2nd order labels, their combination, and a baseline across three fine-grained datasets and one generic dataset (Fig. 7). The results show that 1st order labels consistently achieve the highest accuracy on fine-grained datasets due to their inherently rich part-level information, which remains effective after downsampling. In contrast, 2nd order labels, though detailed, suffer reduced performance on fine-grained datasets because downsampling limits the number of patches per label. However, on generic datasets like ImageNet-100, 2nd order labels outperform 1st order labels by providing more fine-grained information per sample, where 1st order labels lack sufficient detail. These findings highlight the importance of selecting the appropriate order level based on dataset characteristics, demonstrating PartCo's flexibility in various scenarios.
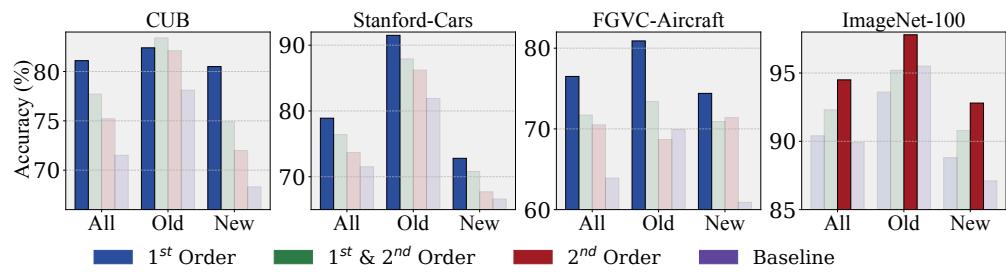

Figure 7: Ablation study investigating the impact of different order levels in part-level correspondence labels. Highest All *ACC* is emphasized, while lower All *ACC* are displayed with reduced opacity.

Impact of output dimensions on part-level projection.
We conduct an ablation study to evaluate the impact of different output dimension sizes for part-level projections ψ_p within our PartCo framework, as shown in Tab. 3. The results indicate that an output dimension d' of 128 consistently yields the best performance across the CUB and Stanford-Cars datasets, achieving the highest accuracy in the overall category metric.

Table 3: Ablation study on part-level projection output dimensions.

	CUB			Stanford-Cars		
Dim.	All	Old	New	All	Old	New
64	79.3	76.7	80.6	76.9	88.3	71.4
128	**81.1**	82.4	80.5	**78.9**	91.5	72.8
256	79.8	80.7	79.4	76.4	90.5	69.7
512	78.2	83.1	75.7	75.6	87.5	69.9

Effect of unsupervised part-level correspondence loss. In addition to the supervised part-level correspondence loss, $\mathcal{L}_{pc}^{sup}$, we conduct an ablation study on PartCo-SimGCD to evaluate the effectiveness of the unsupervised part-level correspondence loss, $\mathcal{L}_{pc}^{unsup}$. As demonstrated in Fig. 8, incorporating $\mathcal{L}_{pc}^{unsup}$ leads to significant improvements in category performance across datasets, highlighting the versatility and robustness of our additional loss when combined with SimGCD.

Figure 8: Impact of the unsupervised part-level correspondence loss ($\mathcal{L}_{pc}^{unsup}$).

Part-level learning boosts category discovery. We assess how part-level learning improves GCD by adding (i) an implicit part learner (SPTNet (Wang et al., 2024)) and (ii) our explicit framework (PartCo) to the SimGCD baseline (Wen et al., 2023) with DINOv2. Results on CUB and Stanford-Cars datasets are summarized in Tab. 4.

Table 4: **Implicit vs. explicit part-level learning.** Study on implicit (SPTNet) and explicit (PartCo) part-level learning frameworks on baseline parametric model: SimGCD.

SimGCD baseline		CUB			Stanford-Cars		
+ PartCo (**Ours**)	+ SPTNet	All	Old	New	All	Old	New
✗	✗	71.5	78.1	68.3	71.5	81.9	66.6
✗	✔	76.3	79.5	74.6	-	-	-
✔	✗	81.1	**82.4**	80.5	78.9	91.5	72.8
✔	✔	**82.6**	82.3	**81.8**	**80.1**	**92.0**	**73.5**

As demonstrated, both approaches provide clear benefits. Adding SPTNet to SimGCD improves the overall accuracy. Using PartCo alone brings larger gains (81.1% on CUB; 78.9% on Stanford-Cars). Combining SPTNet with PartCo outperforms other methods, indicating strong complementarity: implicit cues from SPTNet and explicit part constraints from PartCo enhance feature quality and category separation in distinct ways. In summary, our explicit PartCo not only outperforms the baseline and the implicit SPTNet on its own, but also further amplifies the gains of the implicit framework when combined, underscoring that explicit part learning provides complementary supervision that unlocks additional improvements in category discovery.

5 RELATED WORK

Semi-Supervised Learning (SSL). SSL aims at learning a classifier using both labeled and unlabeled data (Chapelle et al., 2009; Zhu, 2005; Oliver et al., 2018). Most works in this domain assume that the unlabeled data contains instances from the *same* categories in the labeled data (Oliver et al., 2018). Pseudo-labeling (Rizve et al., 2021), consistency regularization (Laine & Aila, 2017; Tarvainen & Valpola, 2017; Berthelot et al., 2019; Sohn et al., 2020), and non-parametric classification (Assran et al., 2021) are among the popular methods for SSL. Most recent works further remove the assumption on the categories in the unlabeled and labeled set, (Saito et al., 2021; Huang et al., 2021; Yu et al., 2020), yet their focus is still on the performance in the labeled set.

Feature descriptors with vision foundation models. Recent ViT models, particularly the DINO variants (Caron et al., 2021; Oquab et al., 2024; Siméoni et al., 2025), have advanced the generation of semantically meaningful and spatially coherent features for dense visual descriptors (Amir et al., 2022). Building on DINOv1 (Caron et al., 2021), DINOv2 (Oquab et al., 2024) scales up the model

size and incorporates a larger curated dataset, enhancing generalization in correspondence tasks such as part-level segmentation and zero-shot semantic correspondence (Zhang et al., 2023).

Part-level learning and semantic correspondence. Supervised fine-grained pipelines use annotated parts to normalize pose and reduce intraclass variance (Branson et al., 2014), and parts can be transferred between categories with reduced labels (Novotny et al., 2016). To reduce annotation cost, weakly / self-supervised methods learn dense features sensitive to geometry or geometrically stable for semantic matching (Novotny et al., 2017; 2018), while unsupervised approaches induce parts through shape-appearance disentangling or contrastive reconstruction (Lorenz et al., 2019; Choudhury et al., 2021). Cross-category canonicalization learns shared dense geometry without manual inter-category links (Neverova et al., 2021), and open-vocabulary part segmentation scales part reasoning using vision–language supervision and DINO-style descriptors (Sun et al., 2023; Choi et al., 2025). Unlike these lines that focused on part alignment or segmentation, we study *Generalized Category Discovery* (GCD), where a small labeled subset (known classes) coexists with unlabeled data containing both known and novel classes. Prior part-based methods typically assume part/keypoint labels (Novotny et al., 2016) or optimize matching-specific objectives (Novotny et al., 2017); while AnchorNet transfers to unseen classes for matching (Novotny et al., 2017), these works do not discover or cluster unknown categories without labels. In contrast, *PartCo distills part-level observations* into GCD via a tailored correspondence loss, yielding robust, part-aware features under mixed supervision and enabling semantically coherent clusters for unseen categories without part annotations or open-vocabulary text labels, while benefiting from the explicit inductive biases revealed by part-level correspondences.

Category Discovery. Novel Class Discovery (NCD) (Han et al., 2019) facilitates knowledge transfer from known to unseen categories through transfer clustering. Since its introduction, various methods are developed to advance NCD (Han et al., 2020; 2021; Jia et al., 2021; Zhao & Han, 2021; Zhong et al., 2021; Fini et al., 2021). Generalized Category Discovery (GCD) (Vaze et al., 2022a) extends NCD by incorporating unlabeled data from both known and unknown classes, presenting additional challenges. Subsequent research on GCD proposes diverse strategies to address these complexities (Cao et al., 2022; Joseph et al., 2022; Pu et al., 2023; Hao et al., 2024; Cendra et al., 2024; Wang et al., 2025; Liu & Han, 2025). For example, SimGCD (Wen et al., 2023) introduces a parametric classifier with mean entropy regularization, while GPC (Zhao et al., 2023) utilizes Gaussian mixture models to learn robust representations and estimate the number of unknown categories. SPTNet (Wang et al., 2024) employs spatial prompt tuning to enhance focus on specific object parts, improving knowledge transfer in GCD tasks. Recently, FlipClass (Lin et al., 2024) dynamically updates the teacher model to align with the student's attention, ensuring consistency across all classes, and SelEx (Rastegar et al., 2024) achieves SOTA performance on fine-grained datasets through hierarchical semi-supervised k-means clustering. Additionally, category discovery is explored in various contexts, including multi-modal settings (Jia et al., 2021), continual learning (Zhang et al., 2022; Cendra et al., 2024), federated environments (Pu et al., 2024), and handling domain shifts (Wang et al., 2025). Our work contributes to this body of research by introducing PartCo, which integrates part-level visual feature correspondences to enhance category discovery. This approach not only improves the accuracy and robustness of discovering novel categories but also provides a more nuanced understanding of category relationships through finer-grained semantic structures, offering a novel framework for category discovery.

6 Conclusion

In this paper, we introduced PartCo, a learning framework for GCD by integrating explicit part-level visual feature correspondences. Unlike traditional GCD methods that rely solely on semantic labels, PartCo leverages the detailed composition of object features to improve category understanding and discovery. Our experiments on multiple benchmark datasets demonstrate that our framework significantly boosts existing GCD methods. Its seamless integration with current approaches without major modifications highlights its practicality and broad applicability. By focusing on part-level relationships, PartCo not only increases discovery accuracy but also provides deeper insights into the visual structures underlying semantic labels. Overall, PartCo bridges the gap between semantic labels and part-level feature compositions, setting the new SOTA for GCD.

REFERENCES

Shir Amir, Yossi Gandelsman, Shai Bagon, and Tali Dekel. Deep vit features as dense visual descriptors. In *ECCV workshop*, 2022. 9

Mahmoud Assran, Mathilde Caron, Ishan Misra, Piotr Bojanowski, Armand Joulin, Nicolas Ballas, and Michael Rabbat. Semi-supervised learning of visual features by non-parametrically predicting view assignments with support samples. In *ICCV*, 2021. 9

Anwesha Banerjee, Liyana Sahir Kallooriyakath, and Soma Biswas. Amend: Adaptive margin and expanded neighborhood for efficient generalized category discovery. In *WACV*, 2024. 7

David Berthelot, Nicholas Carlini, Ian Goodfellow, Nicolas Papernot, Avital Oliver, and Colin Raffel. Mixmatch: A holistic approach to semi-supervised learning. In *NeurIPS*, 2019. 9

Steve Branson, Grant Van Horn, Serge Belongie, and Pietro Perona. Bird species categorization using pose normalized deep convolutional nets. In *BMVC*, 2014. 10

Kaidi Cao, Maria Brbic, and Jure Leskovec. Open-world semi-supervised learning. In *ICLR*, 2022. 10

Mathilde Caron, Hugo Touvron, Ishan Misra, Herve Jegou, Julien Mairal, Piotr Bojanowski, and Armand Joulin. Emerging properties in self-supervised vision transformers. In *ICCV*, 2021. 2, 3, 9, 19

Fernando Julio Cendra, Bingchen Zhao, and Kai Han. Promptccd: Learning gaussian mixture prompt pool for continual category discovery. In *ECCV*, 2024. 10

Olivier Chapelle, Bernhard Scholkopf, and Alexander Zien. Semi-supervised learning (chapelle, o. et al., eds.; 2006)[book reviews]. *IEEE Transactions on Neural Networks*, 2009. 9

Jiho Choi, Seonho Lee, Minhyun Lee, Seungho Lee, and Hyunjung Shim. Fine-grained image-text correspondence with cost aggregation for open-vocabulary part segmentation. In *CVPR*, 2025. 10

Subhabrata Choudhury, Iro Laina, Christian Rupprecht, and Andrea Vedaldi. Unsupervised part discovery from contrastive reconstruction. In *NeurIPS*, 2021. 10

Jia Deng, Wei Dong, Richard Socher, Li-Jia Li, Kai Li, and Li Fei-Fei. Imagenet: A large-scale hierarchical image database. In *CVPR*, 2009. 7, 16

Alexey Dosovitskiy, Lucas Beyer, Alexander Kolesnikov, Dirk Weissenborn, Xiaohua Zhai, Thomas Unterthiner, Mostafa Dehghani, Matthias Minderer, Georg Heigold, Sylvain Gelly, et al. An image is worth 16x16 words: Transformers for image recognition at scale. In *ICLR*, 2021. 3

Enrico Fini, Enver Sangineto, Stéphane Lathuiliere, Zhun Zhong, Moin Nabi, and Elisa Ricci. A unified objective for novel class discovery. In *ICCV*, 2021. 10

Kai Han, Andrea Vedaldi, and Andrew Zisserman. Learning to discover novel visual categories via deep transfer clustering. In *ICCV*, 2019. 2, 10

Kai Han, Sylvestre-Alvise Rebuffi, Sebastien Ehrhardt, Andrea Vedaldi, and Andrew Zisserman. Automatically discovering and learning new visual categories with ranking statistics. In *ICLR*, 2020. 10

Kai Han, Sylvestre-Alvise Rebuffi, Sebastien Ehrhardt, Andrea Vedaldi, and Andrew Zisserman. Autonovel: Automatically discovering and learning novel visual categories. *IEEE TPAMI*, 2021. 2, 10

Shaozhe Hao, Kai Han, and Kwan-Yee K Wong. Cipr: An efficient framework with cross-instance positive relations for generalized category discovery. *TMLR*, 2024. 7, 10, 18

Junkai Huang, Chaowei Fang, Weikai Chen, Zhenhua Chai, Xiaolin Wei, Pengxu Wei, Liang Lin, and Guanbin Li. Trash to treasure: harvesting ood data with cross-modal matching for open-set semi-supervised learning. In *ICCV*, 2021. 9

Xuhui Jia, Kai Han, Yukun Zhu, and Bradley Green. Joint representation learning and novel category discovery on single-and multi-modal data. In *ICCV*, 2021. 10

KJ Joseph, Sujoy Paul, Gaurav Aggarwal, Soma Biswas, Piyush Rai, Kai Han, and Vineeth N Balasubramanian. Novel class discovery without forgetting. In *ECCV*, 2022. 10

Jonathan Krause, Michael Stark, Jia Deng, and Li Fei-Fei. 3d object representations for fine-grained categorization. In *ICCV workshop*, 2013. 6, 16, 18, 19

A. Krizhevsky and G. Hinton. Learning multiple layers of features from tiny images. *Master's thesis, Department of Computer Science, University of Toronto*, 2009. 7, 16

Samuli Laine and Timo Aila. Temporal ensembling for semi-supervised learning. In *ICLR*, 2017. 9

Haonan Lin, Wenbin An, Jiahao Wang, Yan Chen, Feng Tian, Mengmeng Wang, QianYing Wang, Guang Dai, and Jingdong Wang. Flipped classroom: Aligning teacher attention with student in generalized category discovery. In *NeurIPS*, 2024. 7, 10

Yuanpei Liu and Kai Han. Debgcd: Debiased learning with distribution guidance for generalized category discovery. In *ICLR*, 2025. 10

Dominik Lorenz, Leonard Bereska, Timo Milbich, and Bjorn Ommer. Unsupervised part-based disentangling of object shape and appearance. In *CVPR*, 2019. 10

Shijie Ma, Fei Zhu, Xu-Yao Zhang, and Cheng-Lin Liu. Protogcd: Unified and unbiased prototype learning for generalized category discovery. *IEEE TPAMI*, 2025. 7

Subhransu Maji, Esa Rahtu, Juho Kannala, Matthew Blaschko, and Andrea Vedaldi. Fine-grained visual classification of aircraft. *arXiv preprint arXiv:1306.5151*, 2013. 6, 16

Natalia Neverova, Artsiom Sanakoyeu, Patrick Labatut, David Novotny, and Andrea Vedaldi. Discovering relationships between object categories via universal canonical maps. In *CVPR*, 2021. 10

David Novotny, Diane Larlus, and Andrea Vedaldi. I have seen enough: Transferring parts across categories. In *BMVC*, 2016. 10

David Novotny, Diane Larlus, and Andrea Vedaldi. AnchorNet: A weakly supervised network to learn geometry-sensitive features for semantic matching. In *CVPR*, 2017. 10

David Novotny, Samuel Albanie, Diane Larlus, and Andrea Vedaldi. Self-supervised learning of geometrically stable features through probabilistic introspection. In *CVPR*, 2018. 10

Avital Oliver, Augustus Odena, Colin A Raffel, Ekin Dogus Cubuk, and Ian Goodfellow. Realistic evaluation of deep semi-supervised learning algorithms. In *NeurIPS*, 2018. 9

Maxime Oquab, Timothée Darcet, Théo Moutakanni, Huy V. Vo, Marc Szafraniec, Vasil Khalidov, Pierre Fernandez, Daniel HAZIZA, Francisco Massa, Alaaeldin El-Nouby, Mido Assran, Nicolas Ballas, Wojciech Galuba, Russell Howes, Po-Yao Huang, Shang-Wen Li, Ishan Misra, Michael Rabbat, Vasu Sharma, Gabriel Synnaeve, Hu Xu, Herve Jegou, Julien Mairal, Patrick Labatut, Armand Joulin, and Piotr Bojanowski. DINOv2: Learning robust visual features without supervision. *TMLR*, 2024. 2, 4, 7, 9, 17, 18

Omkar M Parkhi, Andrea Vedaldi, Andrew Zisserman, and CV Jawahar. Cats and dogs. In *CVPR*, 2012. 16, 17

Nan Pu, Zhun Zhong, and Nicu Sebe. Dynamic conceptional contrastive learning for generalized category discovery. In *CVPR*, 2023. 10

Nan Pu, Wenjing Li, Xingyuan Ji, Yalan Qin, Nicu Sebe, and Zhun Zhong. Federated generalized category discovery. In *CVPR*, 2024. 10

Sarah Rastegar, Mohammadreza Salehi, Yuki M Asano, Hazel Doughty, and Cees G M Snoek. Selex: Self-expertise in fine-grained generalized category discovery. In *ECCV*, 2024. 3, 7, 10, 18, 19

Mamshad Nayeem Rizve, Kevin Duarte, Yogesh S Rawat, and Mubarak Shah. In defense of pseudo-labeling: An uncertainty-aware pseudo-label selection framework for semi-supervised learning. In *ICLR*, 2021. 9

Kuniaki Saito, Donghyun Kim, and Kate Saenko. Openmatch: Open-set consistency regularization for semi-supervised learning with outliers. In *NeurIPS*, 2021. 9

Oriane Siméoni, Huy V Vo, Maximilian Seitzer, Federico Baldassarre, Maxime Oquab, Cijo Jose, Vasil Khalidov, Marc Szafraniec, Seungeun Yi, Michaël Ramamonjisoa, et al. Dinov3. *arXiv preprint arXiv:2508.10104*, 2025. 2, 4, 7, 9

Kihyuk Sohn, David Berthelot, Nicholas Carlini, Zizhao Zhang, Han Zhang, Colin A Raffel, Ekin Dogus Cubuk, Alexey Kurakin, and Chun-Liang Li. Fixmatch: Simplifying semi-supervised learning with consistency and confidence. In *NeurIPS*, 2020. 9

Peize Sun, Shoufa Chen, Chenchen Zhu, Fanyi Xiao, Ping Luo, Saining Xie, and Zhicheng Yan. Going denser with open-vocabulary part segmentation. In *ICCV*, 2023. 10

Kiat Chuan Tan, Yulong Liu, Barbara Ambrose, Melissa Tulig, and Serge Belongie. The herbarium challenge 2019 dataset. In *CVPR workshop*, 2019. 16, 17

Antti Tarvainen and Harri Valpola. Mean teachers are better role models: Weight-averaged consistency targets improve semi-supervised deep learning results. In *NeurIPS*, 2017. 9

Sagar Vaze, Kai Han, Andrea Vedaldi, and Andrew Zisserman. Generalized category discovery. In *CVPR*, 2022a. 1, 2, 3, 7, 10, 16, 17, 18

Sagar Vaze, Kai Han, Andrea Vedaldi, and Andrew Zisserman. The semantic shift benchmark. In *ICML workshop*, 2022b. 6

Sagar Vaze, Andrea Vedaldi, and Andrew Zisserman. No representation rules them all in category discovery. In *NeurIPS*, 2023. 2, 7

Catherine Wah, Steve Branson, Peter Welinder, Pietro Perona, and Serge Belongie. The caltech-ucsd birds-200-2011 dataset. *California Institute of Technology*, 2011. 6, 16, 18, 19

Hongjun Wang, Sagar Vaze, and Kai Han. Sptnet: An efficient alternative framework for generalized category discovery with spatial prompt tuning. In *ICLR*, 2024. 2, 7, 9, 10

Hongjun Wang, Sagar Vaze, and Kai Han. Hilo: A learning framework for generalized category discovery robust to domain shifts. In *ICLR*, 2025. 10

Xin Wen, Bingchen Zhao, and Xiaojuan Qi. Parametric classification for generalized category discovery: A baseline study. In *ICCV*, 2023. 3, 7, 9, 10, 19

Qing Yu, Daiki Ikami, Go Irie, and Kiyoharu Aizawa. Multi-task curriculum framework for open-set semi-supervised learning. In *ECCV*, 2020. 9

Junyi Zhang, Charles Herrmann, Junhwa Hur, Luisa Polania Cabrera, Varun Jampani, Deqing Sun, and Ming-Hsuan Yang. A tale of two features: Stable diffusion complements dino for zero-shot semantic correspondence. In *NeurIPS*, 2023. 10, 17

Xinwei Zhang, Jianwen Jiang, Yutong Feng, Zhi-fan Wu, Xibin Zhao, Hai Wan, Mingqian Tang, Rong Jin, and Yue Gao. Grow and merge: a unified framework for continuous categories discovery. In *NeurIPS*, 2022. 10

Bingchen Zhao and Kai Han. Novel visual category discovery with dual ranking statistics and mutual knowledge distillation. In *NeurIPS*, 2021. 10

Bingchen Zhao, Xin Wen, and Kai Han. Learning semi-supervised gaussian mixture models for generalized category discovery. In *ICCV*, 2023. 10, 18

Zhun Zhong, Enrico Fini, Subhankar Roy, Zhiming Luo, Elisa Ricci, and Nicu Sebe. Neighborhood contrastive learning for novel class discovery. In *CVPR*, 2021. 10

Xiaojin Jerry Zhu. Semi-supervised learning literature survey. *University of Wisconsin-Madison Department of Computer Sciences*, 2005. 9

PartCo: Part-Level Correspondence Priors
Enhance Category Discovery
–Supplementary Material–

CONTENTS

S1 ADDITIONAL EXPERIMENTAL DETAILS

S1.1 BENCHMARK DATASETS

For each benchmark dataset, we follow the data splitting approach outlined in Vaze et al. (2022a). In this approach, 50% of the classes are designated as 'Old', except for CIFAR-100, which selects 80% of the classes. Subsequently, 50% of the images from the known classes form the labeled dataset $\mathbf{D}_l$, while the remaining images are assigned to the unlabeled dataset $\mathbf{D}_u$. The statistics of all datasets used in this study are presented in Tab. A.

S1.2 TIME ANALYSIS FOR PART-LEVEL CORRESPONDENCE LABELS CONSTRUCTION

In Sec. 3.1 of the main paper, we describe the methodology for generating part-level correspondence labels. The overall time required to construct these labels for each dataset is detailed in the last column of Tab. A. As illustrated, our label construction process is efficient, with execution times ranging from approximately 5 to 180 minutes depending on the dataset's size and complexity. Importantly, this time cost is negligible compared to typical model training durations, and it is incurred solely during the training phase. Consequently, the label construction does not introduce any additional latency during the inference phase. While it is feasible to integrate the label construction directly into the training pipeline, we have opted to separate these steps to simplify the implementation and facilitate easier experimentation.

Table A: **Dataset statistics.** We specify the number of classes in the labeled and unlabeled sets as $M = |\mathbf{Y}_l|$ and $K = |\mathbf{Y}_l \cup \mathbf{Y}_u|$, respectively, along with the image counts $|\mathbf{D}_l|$ and $|\mathbf{D}_u|$. In the last column, we also provide the time taken (minutes) to construct PartCo's labels.

Dataset	$|\mathbf{D}_l|$	M	$|\mathbf{D}_u|$	K	PartCo label time (min)
CUB (Wah et al., 2011)	1.5K	100	4.5K	200	6 min
Stanford-Cars (Krause et al., 2013)	2.0K	98	6.1K	196	5 min
FGVC-Aircraft (Maji et al., 2013)	1.7K	50	5.0K	100	7 min
CIFAR10 (Krizhevsky & Hinton, 2009)	12.5K	5	37.5K	10	30 min
CIFAR100 (Krizhevsky & Hinton, 2009)	20.0K	80	30.0K	100	30 min
ImageNet-100 (Deng et al., 2009)	31.9K	50	95.3K	100	180 min
Oxford-Pet (Parkhi et al., 2012)	0.9K	19	2.7K	37	5 min
Herbarium19 (Tan et al., 2019)	8.9K	341	25.4K	683	118 min

S2 Additional Quantitative Results

S2.1 Experiments on additional datasets

To further assess the effectiveness of our PartCo framework, we conducted evaluations on two additional fine-grained datasets: Oxford-Pet (Parkhi et al., 2012) and Herbarium19 (Tan et al., 2019). The Oxford-Pet dataset is particularly challenging due to its diverse assortment of cat and dog species combined with limited data availability. In contrast, Herbarium19 is a botanical research dataset that includes a wide variety of plant types, characterized by its long-tailed distribution and detailed categorization. The details of these two datasets are shown in Tab. A.

As shown in Tab. B, our PartCo-enhanced models consistently outperform the baseline method across all categories. Specifically, PartCo-SimGCD achieves an impressive accuracy of 95.2% on the 'All' category of the Oxford-Pet dataset, significantly surpassing the SimGCD baseline's 86.2%. Similarly, on the Herbarium19 dataset, PartCo-SimGCD attains an accuracy of 55.5%, outperforming the baseline's 48.6%. Overall, these results demonstrate that our PartCo framework effectively enhances existing baseline models, even when applied to more challenging fine-grained and long-tailed datasets.

Table B: **Enhancement of baseline GCD methods with PartCo framework.** Performance on the Oxford-Pet (Parkhi et al., 2012) and Herbarium19 (Tan et al., 2019) datasets using DINOv2. Results are reported in *ACC* across the 'All', 'Old' and 'New' categories.

Method	Oxford-Pet			Herbarium19		
	All	Old	New	All	Old	New
SimGCD	86.2	85.4	86.6	48.6	64.8	39.9
PartCo-SimGCD (Ours)	**95.2**	**92.7**	**96.6**	**55.5**	**68.0**	**48.7**

S2.2 Comparison of different approaches for part-level label construction

In this work, we use PCA + DINOv2 (Oquab et al., 2024) features for the following reasons: **(1) Generalization.** PCA with DINOv2 offers excellent off-the-shelf generalization for generating part-level correspondences without the need for additional tuning or adaptation. According to Zhang et al. (2023), DINOv2 outperforms other foundation models like DINO and Stable Diffusion (SD) models, and is only slightly less effective than combining DINOv2 + SD. **(2) Efficiency.** Incorporating SD-based features, or a combination of SD and DINO-based models, significantly increases computational costs and memory usage (Zhang et al., 2023). This makes the part-label construction process inefficient. By using DINOv2 solely, our approach remains both computationally and model-efficient.

Moreover, we construct labels by augmenting DINOv2 features with SD features to compute PCA, following Zhang et al. (2023). Because SD requires an inference denoising step, this procedure is computationally heavy: on CUB it takes around 108 minutes, whereas our PCA + DINOv2 pipeline takes around 6 minutes (Tab. A, supp. material), making SD-DINOv2 impractical for larger datasets (e.g., ImageNet-100). We further compared performance using SD-DINOv2-based labels against our original labels. As shown in Tab. C, the 'All' *ACC* differences are marginal (about 0.2–0.6 percentage points) while our PCA + DINOv2 label construction is substantially faster and more efficient.

Table C: **Influence of different part-level correspondence labels construction techniques.** Performance on the CUB and Stanford-Cars datasets with different part-level correspondence labels generated by Our method vs. SD-DINOv2 (Zhang et al., 2023). Results are reported in *ACC* across the 'All', 'Old' and 'New' categories.

PartCo-SimGCD	CUB			Stanford-Cars		
	All	Old	New	All	Old	New
w/ DINOv2 **(Ours)**	81.1	82.4	80.5	78.9	91.5	72.8
w/ SD-DINOv2	80.9	79.7	81.6	78.3	90.0	72.9

S2.3 Study on unknown category estimation methods

In the real-world category discovery task, the exact number of novel categories is often unknown, posing a significant challenge for model training and evaluation. Existing literature (Vaze et al.,

2022a; Hao et al., 2024; Zhao et al., 2023), has explored methods to estimate the number of unknown categories (K). Building upon these studies, we conduct a comprehensive analysis to assess the effectiveness of different K-estimation methods when integrated with a stronger foundation model, specifically DINOv2 (Oquab et al., 2024).

Our experimental setup involves training three distinct GCD methods, *i.e.*, GCD (Vaze et al., 2022a), SelEx (Rastegar et al., 2024), and our proposed PartCo-SelEx (Ours) using DINOv2 pretrained weights. These trained models serve as feature extractors for the subsequent K-estimation process. We employ two off-the-shelf K-estimation techniques: GCD (Vaze et al., 2022a) and CiPR (Hao et al., 2024) K-est methods. The performance of these integrated approaches is evaluated on two fine-grained datasets: CUB (Wah et al., 2011) and Stanford-Cars (Krause et al., 2013).

Table D: **Unknown category estimation.** Category estimation results of various K-estimation methods on different GCD methods using DINOv2.

	CUB		Stanford-Cars	
Method	GCD K-est	CiPR K-est	GCD K-est	CiPR K-est
GCD	188	178	242	169
SelEx	219	191	229	194
PartCo-SelEx (Ours)	210	192	185	195
Ground-truth K	200		196	

Tab. D shows the estimation results of different K-estimation methods when applied to the GCD, SelEx, and PartCo-SelEx methods. The ground-truth number of categories is 200 for the CUB dataset and 196 for the Stanford-Cars dataset. We observe that the GCD K-estimation method, when paired with the GCD's weights, significantly underestimates $K = 188$ for CUB dataset and overestimates $K = 242$ for Stanford-Cars. In contrast, the CiPR K-estimation method offers improved estimations, though still not perfectly aligned with the ground truth ($K = 178$ for CUB and $K = 169$ for Stanford-Cars).

When integrating SelEx with the K-estimation methods, the performance improves, with CiPR providing more accurate estimates ($K = 191$ for CUB and $K = 194$ for Stanford-Cars) compared to GCD's native method ($K = 219$ for CUB and $K = 229$ for Stanford-Cars). On the other hand, our proposed PartCo-SelEx framework demonstrates the most accurate K-estimation across both datasets, achieving estimates of 210 for CUB and 185 for Stanford-Cars with the GCD K-estimation method, and $K = 192$ for CUB and $K = 195$ for Stanford-Cars with the CiPR method. These results indicate that PartCo-SelEx consistently provides K-estimates that are closer to the ground truth, particularly when using the CiPR estimation method.

Table E: **GCD performance with estimated K.** GCD results on DINOv2 with the estimated number of categories.

	CUB			Stanford-Cars		
Method	All	Old	New	All	Old	New
GCD	68.9	77.0	65.0	62.2	72.5	57.2
SimGCD	70.4	78.1	66.7	69.7	84.8	62.3
PartCo-SimGCD (Ours)	78.8	**80.3**	78.0	73.9	84.9	68.6
SelEx	86.1	77.8	90.3	78.3	**89.2**	73.0
PartCo-SelEx (Ours)	**87.6**	79.3	**91.7**	**80.6**	88.7	**76.8**

To further evaluate the robustness of our method under challenging K-estimation scenarios, we conduct experiments using the worst estimation method results: $K = 188$ for CUB and $K = 242$ for Stanford-Cars, as shown in Tab. E. Despite these inaccurate K-estimates, our PartCo-SelEx framework maintains superior performance compared to baseline models. Specifically, on the CUB dataset, PartCo-SelEx achieves an accuracy of 87.6% on the 'All' category and 91.7% on the 'New' category, outperforming the SelEx baseline which achieves 86.1% and 90.3% respectively. Similarly, on the Stanford-Cars dataset, PartCo-SelEx attains the highest accuracies of 80.6% for 'All' and 76.8% for 'New' categories, surpassing the SelEx baseline's 78.3% and 73.0% respectively. These results underscore the robustness of PartCo-SelEx in handling erroneous K-estimates, ensuring consistent and reliable performance even when the estimated number of categories deviates from the ground truth.

S3 Qualitative Results

S3.1 Additional visualization of part-level correspondence labels
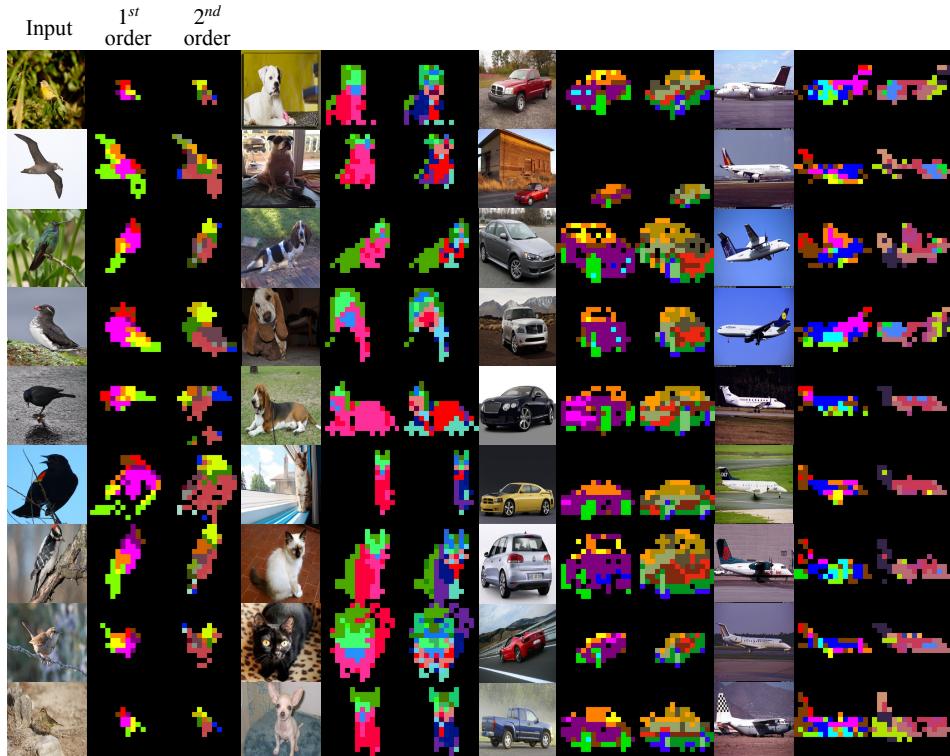

Figure A: **Additional visualization of our part-level correspondence labels.** For every input image, both first and second-order labels are constructed.

S3.2 Qualitative analysis of PartCo attention maps

We provide a qualitative analysis of the attention maps generated by SimGCD (Wen et al., 2023) and SelEx (Rastegar et al., 2024) when integrated with the PartCo framework (Ours), applied to the CUB (Wah et al., 2011) and Stanford-Cars (Krause et al., 2013) datasets, as shown in Fig. B & C. These attention maps originate from the final block of DINOv2 ViT backbone, utilizing a resolution of 16×16. Following the methodology outlined in Caron et al. (2021), we calculate the mean value across all attention heads and upsample the resulting maps to the original image resolution for visualization purposes. The analysis shows that all evaluated methods focus their attention on specific parts of the objects, effectively highlighting regions crucial for distinguishing between fine-grained categories. Notably, when combined with SimGCD, the PartCo framework (PartCo-SimGCD) tends to concentrate on particular parts of the object, such as the wings of a bird in the CUB dataset or the wheels of a car in the Stanford-Cars dataset. This targeted focus underscores PartCo-SimGCD's ability to hone in on key discriminative features essential for accurate category differentiation. In contrast, integrating PartCo with SelEx (PartCo-SelEx) results in attention maps that cover a broader range of object parts, capturing multiple fine-grained details simultaneously. For example, PartCo-SelEx not only highlights the wings but also the body and head of the bird in the CUB dataset, and the wheels, doors, and headlights of the car in the Stanford-Cars dataset.

These observations indicate that while both PartCo-SimGCD and PartCo-SelEx effectively utilize part-level information to enhance attention mechanisms, PartCo-SelEx exhibits a more comprehensive focus on multiple object parts. This broader attention coverage can potentially lead to a more nuanced understanding of fine-grained categories, thereby improving the model's ability to generalize across diverse and complex datasets. Overall, the qualitative analysis demonstrates the robustness and effectiveness of the PartCo framework in refining attention maps, highlighting its superior capability to capture meaningful visual regions.
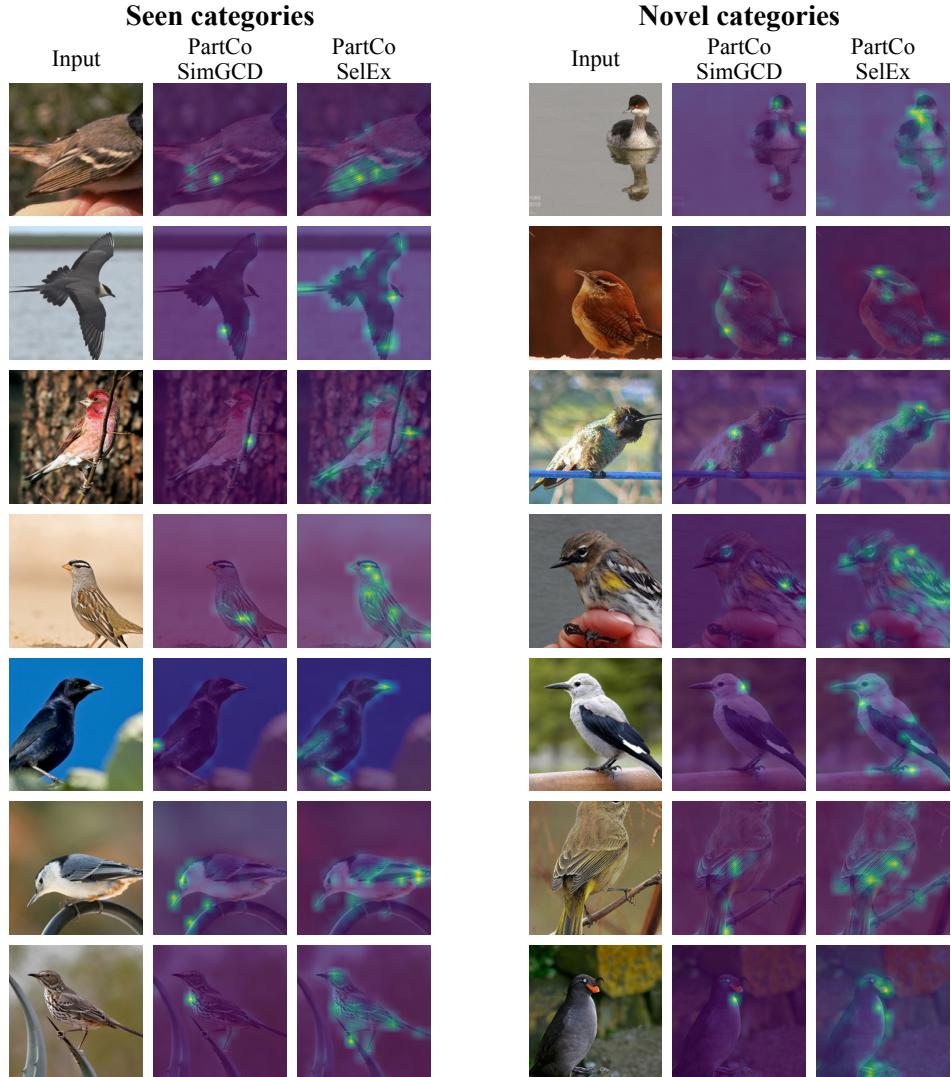
Figure B: **Attention maps on CUB dataset.** Visualization of attention maps generated by the PartCo framework integrated with SimGCD and SelEx for the CUB dataset. The PartCo-SimGCD model highlights specific regions such as the wings and head of the bird, indicating focused attention on key discriminative features. In contrast, the PartCo-SelEx model displays a broader attention distribution, encompassing multiple parts including the wings, body, and tail.

Figure C: **Attention maps on Stanford-Cars dataset.** Visualization of attention maps generated by the PartCo framework integrated with SimGCD and SelEx for the Stanford-Cars dataset. The PartCo-SimGCD model concentrates on distinct parts like the wheels and headlights of the car, demonstrating targeted attention on essential distinguishing features. Meanwhile, the PartCo-SelEx model exhibits a wider area of focus, covering various components such as the wheels, doors, and overall body structure.

S4 LIMITATIONS

The PartCo framework currently relies on foundation models that provide patch token representations, which are characteristic of recent transformer-based architectures. This dependence makes PartCo incompatible with models that lack patch tokens, such as certain convolutional neural networks and older architectures, thereby limiting its generalizability. Future research should focus on developing methods to integrate part-level or localized information into PartCo, allowing it to be effectively applied across a broader range of foundation models.

S5 BROADER IMPACTS

The development of the Part-Level Correspondence Prior (PartCo) framework represents a significant advancement in category discovery, especially in recognizing fine-grained categories and enabling more robust intelligent systems in real-world scenarios. Fine-grained category recognition is essential in fields such as biodiversity conservation, where precise species identification supports ecological monitoring, and in healthcare, where detailed analysis of medical images could potentially lead to improved disease diagnosis and personalized treatment plans. However, the deployment of PartCo also presents potential ethical and societal challenges. Enhanced image recognition capabilities could be misused in surveillance systems, raising significant privacy concerns. There is a risk that biased training data may lead to unfair or discriminatory outcomes. To mitigate these risks, it is essential to implement robust data governance frameworks that ensure diversity and representativeness in training datasets, thereby minimizing biases. Privacy-preserving techniques and strict regulatory compliance should be prioritized to protect individual rights and prevent misuse in categorization tasks.